Publication I

Olli Himanen, Tero Hottinen, Mikko Mikkola, Ville Saarinen, "*Characterization of membrane electrode assembly with hydrogen-hydrogen cell and ac-impedance spectroscopy Part I. Experimental*", Electrochimica Acta 52, pp. 206-214, 2006

Available online at www.sciencedirect.com
ScienceDirect
Electrochimica Acta 52 (2006) 206–214
ELECTROCHIMICA Acta
www.elsevier.com/locate/electacta

Characterization of membrane electrode assembly with hydrogen–hydrogen cell and ac-impedance spectroscopy Part I. Experimental

Olli Himanen [a,*], Tero Hottinen [a], Mikko Mikkola [a], Ville Saarinen [b]

[a] *Helsinki University of Technology, Laboratory of Advanced Energy Systems, P.O. Box 2200, 02015 HUT, Finland*
[b] *Helsinki University of Technology, Laboratory of Physical Chemistry and Electrochemistry, P.O. Box 6100, 02015 HUT, Finland*

Received 18 January 2006; received in revised form 2 May 2006; accepted 2 May 2006
Available online 30 June 2006

Abstract

A measurement system based on a symmetrical hydrogen–hydrogen cell was developed and presented. The net water flux through and impedance of Gore™ Primea® Series 58 MEA were measured under different humidity conditions. An equivalent circuit approach was used to analyze impedance measurement data and the dependences of membrane conductivity and reaction kinetics on the humidity were obtained. Modeling work was found necessary to estimate the diffusion coefficient of water in the membrane, because humidity profile inside the cell was uneven and unknown during the net water flux measurements. Gas permeabilities of different cell components and water uptake of the MEA were measured to get parameter values for the modeling work. The actual modeling work was not conducted in this contribution, but is explained in Part II of this paper.

Keywords: PEMFC; Hydrogen–hydrogen cell; Water transport; Hydraulic permeability; Water uptake

1. Introduction

Water management is one of the key factors affecting the performance of polymer electrolyte membrane fuel cells. The conductivity of perfluorosulfonic acid membranes increases with the water content of the membrane. On the other hand, excess water may cover reaction sites on the electrodes and hinder reactant flow, which decreases the performance of the cell.

In this work, the effect of humidity on water transport and electrochemical properties of a commercial membrane electrode assembly (MEA), Gore™ Primea® Series 58, was studied experimentally and theoretically. The report is divided into two parts; this part explains the experimental details and measurement results. Part II [1] introduces theoretical models that are used to analyze the measurement results. As a result of the modeling work explained in Ref. [1], the dependence of the diffusion coefficient of water in the membrane on the water content is achieved.

In situ measurements explained in this part were conducted with a hydrogen–hydrogen cell (H_2–H_2 cell). The membrane conductivity and anode side reaction kinetics were determined with ac-impedance spectroscopy. The net water flux through the membrane was evaluated from the measured humidities of ingoing and exiting gas streams. The water uptake (WU) of the MEA and the hydraulic permeabilities of different cell components were also measured to get parameters for the modeling work.

The H_2–H_2 cell is typically used as a hydrogen compressor or purifier, but it also has potential to be used as a tool in PEMFC research. The components of H_2–H_2 cell are the same as in a PEMFC and especially the transport phenomena in the polymer membrane are identical. One difference between H_2–H_2 cell and PEMFC is that there is no reaction product water in H_2–H_2 cell, and therefore the humidity levels on both sides of the cell can be accurately controlled by the inlet gas humidification. This enables the measurement of diffusive water flux through the membrane. In addition, the total activation losses of H_2–H_2 reactions, given in Eq. (1a) and (1b) Eq. (1), are significantly smaller than in PEMFC, leading to decreased heat production. Smaller heat production makes it possible to treat

DOI of original article:10.1016/j.electacta.2006.05.037.
* Corresponding author.
E-mail address: olli.himanen@tkk.fi (O. Himanen).

0013-4686/$ – see front matter © 2006 Elsevier Ltd. All rights reserved.
doi:10.1016/j.electacta.2006.05.016

H_2–H_2 cell as an isothermal system, which is shown in Ref. [1].

$$H_2 \rightarrow 2H^+ + 2e^- \quad \text{anode} \tag{1a}$$

$$2H^+ + 2e^- \rightarrow H_2 \quad \text{cathode} \tag{1b}$$

H_2–H_2 cell has been previously used to study the anode side reaction kinetics of PEMFC and especially the effect of carbon monoxide, see e.g. [2] and [3]. Matic et al. [4] used H_2–H_2 cell and Raman spectroscopy to study water distribution inside a Nafion® 117 membrane as a function of current density. The use of H_2–H_2 cell as an electrochemical hydrogen compressor has been studied e.g. in Ref. [5].

2. Experimental arrangements

2.1. Measurement system

The measurements were conducted with a symmetrical H_2–H_2 cell by feeding humidified hydrogen into the cell, the humidity levels of both sides of the cell were controlled independently. The humidity levels of the exhaust gases and the impedance spectrum of the MEA were measured under various humidification conditions. The humidity levels of the exiting gases depend on the water flux through the membrane and therefore can be used to determine the diffusion coefficient of water in the membrane. The conductivity of the membrane and the parameters of reaction kinetics can be estimated from the results of impedance measurements.

The measurements were conducted with a similar measurement cell as reported in Ref. [6–8] with slight modifications. It was noticed during the preliminary measurements [9] that with a circular active area of 30 mm diameter, the measured humidities of the exiting gases were equal despite the difference between the humidities at the inlets. When the humidities of outlet gases are equal, there is no concentration gradient of water near the outlets. This means that there is no driving force for water diffusion through the membrane near the outlets. Therefore, water flux through the membrane is zero near the outlets, but it is impossible to say how large this area is. Thus the area for water diffusion was not known. In order to decrease the total water flux through the membrane and to increase the cell impedance, the diameter of the active area was reduced from 30 to 10 mm. In addition, the current collector with a machined spiral flow channel was replaced with a gold-plated AISI 316 steel net on top of a smooth graphite current collector. The openings of the net were 0.415 mm and the thickness of the wire was 0.22 mm. The net was used to create radially symmetric velocity and concentration profiles into the cell. The flow geometry and cell structure are illustrated in Fig. 1. The material of the cell body was PEEK and current collectors were made of ISEM-3 graphite. Planar gaskets were made of 0.22 mm thick glass fiber reinforced PTFE. Gas diffusion backings were SGL ®Sigracet GDL 10-BA. MEA used in this work was GORE™ PRIMEA® Series 58 MEA. The temperature of the cell was controlled with a West 6100 controller, a K-type thermocouple and Watlow EB heating cartridges. The temperature of the cell was measured from the current collector.

Brooks 5850S mass flow controllers, a HP 75000 Series B datalogger and Agilent VEE Pro 6.1 software were used to control the mass flows of dry hydrogen. Hydrogen was humidified in a Fuel Cell Technologies gas humidification unit. The humidification temperatures were chosen so that there were measurement points both in one- and two-phase regions. The temperatures of the gas lines were controlled with West 6100 controller, Horst heating cables and K-type thermocouple.

To determine the humidity level of the exiting hydrogen, the exhaust gas lines were connected to dehydrator pipes filled with Indicating Drierite® desiccant (W.A. Hammond DRIERITE Co., Ltd.). The amount of water exiting the cell on each side was calculated from the weight increase of the desiccant after the experiment. The remaining moisture in gas dried with Indicating Drierite® at room temperature is 5 mg m^{-3} [10], corresponding to a relative humidity of 0.02%. The remaining moisture was not taken into account in the calculation of humidity levels.

The ac-impedance spectra of the MEA were recorded with a Zahner IM6 Electrochemical Workstation and Zahner PP240 potentiostat. IM6 and PP240 were controlled with Thales software made by Zahner. Potentials on the electrode surfaces were measured from inactive areas with 100 μm gold wires. Spectrum analyzer software included in the Thales package was used to

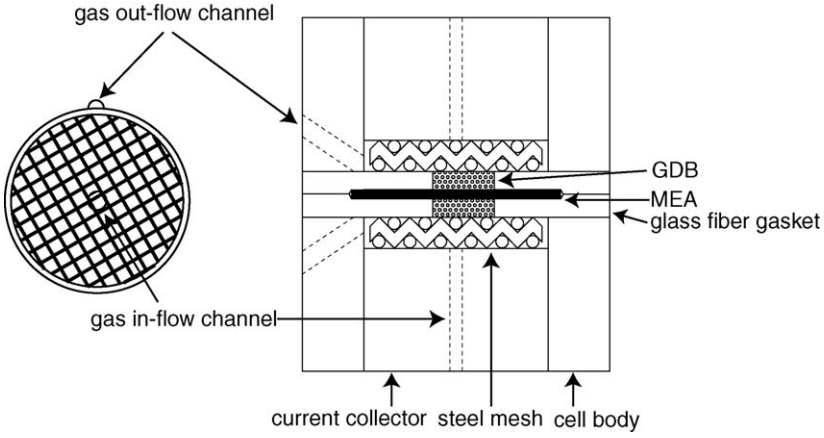

Fig. 1. Flow field geometry and cell structure. Gas channels are marked with dotted lines. The picture is not in scale.

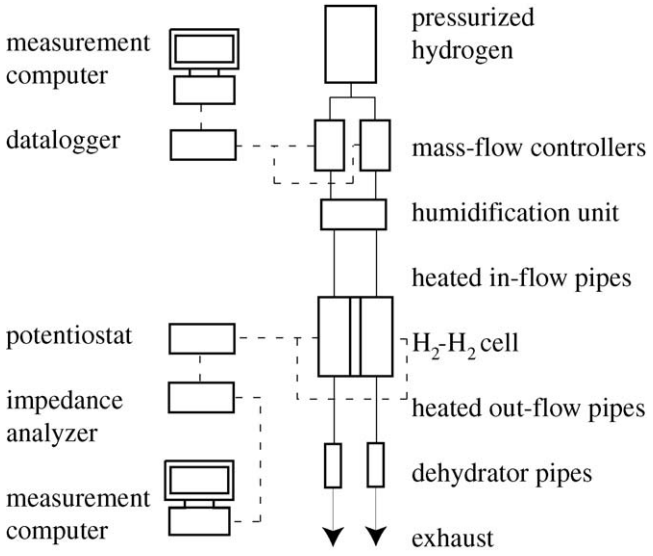

Fig. 2. Measurement system. Electrical and communication wires are denoted with dashed lines and gas pipes with solid lines.

verify that the response of the measured system was linear. A schematic of the measurement system is illustrated in Fig. 2.

Before the H_2–H_2 measurements, the cell was operated in a fuel cell mode to check the gas tightness and to break in the MEA. The cell was operated at 0.38 A cm^{-2} current density for 3 h on dry hydrogen and oxygen, after which a polarization curve was recorded. Subsequently, the cell was purged with nitrogen and anode and cathode were reversed, and the cell was again operated for 3 h at 0.38 A cm^{-2} current density before the second polarization curve measurement. This procedure was repeated until the cell performance stabilized, usually three times. After the break in, the cell was purged with nitrogen and H_2–H_2 measurements were started.

The measurements were conducted at the cell temperature of 35 °C. This temperature was chosen, because it is a typical operating temperature of small unheated PEMFCs, see e.g. [11,12]. The MEA used in this work does not need external humidification and is therefore suitable for use in small PEMFCs.

2.2. Water transport measurements

Measurements were made by varying the humidities of inlet gases and measuring the humidities of exiting gases. Before measurement, the cell was let to stabilize with humidity conditions for at least 4 h. Each measurement condition was measured at least two times. The duration of each measurement was approximately 3 h. Volume flow of dry hydrogen was 250 ml min^{-1} for both sides of the cell. Both sides of the cell were unpressurized.

2.3. Calibration of the humidification system

In order to calculate the total water flux through the membrane, the humidity levels of gases entering the cell must be known with an adequate accuracy. Therefore, the humidity levels of out-coming gases from the humidification system were measured before starting the measurements with H_2–H_2 cell. Each set-point was measured three times and the duration of each measurement was approximately 3 h. The concentration of water in the inlet gas flow was calculated from the weight increase of the desiccant.

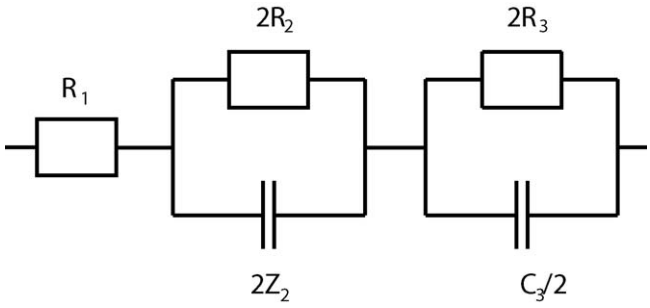

Fig. 3. Equivalent circuit for MEA impedance.

2.4. Impedance model of the MEA

The most common way to analyze impedance data is to fit the parameters of an equivalent circuit into the measured impedance spectrum. Every component of the circuit should have its physical counterpart, e.g. membrane resistance or double layer capacitance. The theoretical model for the MEA impedance used in this work is based on the equivalent circuit illustrated in Fig. 3.

The components of the equivalent circuit are a single resistor, a resistor–capacitor pair and a resistor-constant phase element pair. This kind of equivalent circuit was chosen, because it is the simplest circuit that can physically explain the measured impedance behaviour of the cell. Resistor R_1 is used to describe the pure resistance between the potential probes, which is assumed to be caused by the membrane resistance. R_2 and Z_2 are used to describe charge transfer processes of adsorbed hydrogen, and they define the high frequency arc of the Nyquist plot. R_2 is the charge transfer resistance and Z_2 is the constant phase element. The constant phase element is used instead of a normal capacitor because of capacitance dispersion caused by electrode roughness, see e.g. [13,14]. The impedance of a constant phase element can be calculated with equation

$$Z_{\mathrm{CPE}} = \frac{1}{T(2\pi f)^{\alpha}} \tag{2}$$

The double layer capacitance can be calculated from the constant phase element with equation

$$C_{\mathrm{DL}} = T(2\pi f_{\max})^{\alpha-1}, \tag{3}$$

where $f_{\max}$ is the frequency at which the imaginary component of impedance reaches its maximum, see e.g. [15].

R_3 and C_3 are used to describe adsorption and desorption of hydrogen on the electrode surface and they define the low frequency arc of the Nyquist plot. Alternatively R_3 and C_3 could be caused by the hydrogen diffusion, but Ciureanu and Wang [16] discovered that the low frequency arc was not dependent on the hydrogen flow rate and they concluded that it was not associated with H_2 diffusion.

In order to make the equivalent circuit more accurate, there should be four constant phase element-resistor pairs, one for each reaction. This would make the fitting procedure very challenging and dependent on the initial guess, and therefore the above-described simpler equivalent circuit was used. Both adsorption/desorption and oxidation/reduction reactions are described by one component pair, each. Therefore, there are two component pairs, $2R_2 - 2Z_2$, and $2R_3 - C_3/2$, instead of four component pairs.

2.5. Water uptake measurements

The WU of the GORE™ PRIMEA® Series 58 MEA at 35 °C was measured from water vapor and from liquid water. The water uptake from water vapor was measured using saturated salt solutions to create constant humidity conditions. MEAs were dried with P_2O_5 and then stabilized with water vapor or liquid water at least a week. Surface water was removed from the electrode surfaces with bibulous paper before weighing the MEA stabilized with liquid water. The water uptake was calculated from the weight increase of the MEA.

2.6. Gas permeability measurements

The in-plane gas permeability of gas distributor nets, gas diffusion backings (SGL ®Sigracet GDL 10-BA) and electrodes of GORE™ PRIMEA® Series 58 MEA were measured to obtain parameter values for modeling. The measurement system is illustrated in Fig. 4. The gas permeabilities were measured by forcing a gas flow through circular samples and measuring the pressure difference between the inlet and ambient air. The diameters of the samples and the inlet channel were 63 and 20 mm, respectively. Sample thicknesses were controlled with clearance gauges. The permeability of porous electrodes was measured with two different methods. In the first measurement there was a 10 mm hole in the centre of the MEA sample. This allowed the gas to flow in both electrodes. In the second measurement there was no hole and gas was assumed to flow only inside one electrode. These two methods were used to eliminate the possible errors caused by gas flow through and along the membrane.

3. Results and discussion

3.1. Water transport measurements

The measurement conditions and results of water transport measurements are given in Table 1. The cell sides are called side 1 and side 2. Dew-point is the setting value of the humidification temperature. Inlet concentrations are concentrations of water vapor fed into the cell and they are calculated from the results of calibration measurements. The outlet concentrations refer to the concentrations of water vapor in the gases coming out from the cell. The error estimates for inlet and outlet concentrations are calculated using the largest relative standard deviation among the measurement points, which was 2% for calibration measurements and 5% for water transport measurements. The average water fluxes $\dot{m}_{H_2O}$ through the membrane and their error estimates are also given in Table 1. There was no water concentration gradient in the measurements 15–20, and therefore only the impedance of the MEA was measured.

As expected, the calculated average water fluxes through the membrane are largest under the conditions in which the concentration gradient of water is largest. The largest average diffusive water flux was 11.9×10^{-4} kg m^{-2} s^{-1}, which corresponds to the water flux produced with an average current density of 12800 A m^{-2} in the case of a PEMFC. The error estimates of the water fluxes are quite large, from 8 to 180%, due to the fact that the water flux through the membrane is small compared to the total amount of water fed into the cell. Therefore, even small errors in the determination of the humidity of in-going or exiting gases lead into significant errors in the calculated water flux through the membrane.

The accuracy of the measurements could be improved by increasing the number of repeated measurements, lengthening the measuring periods, and also increasing the accuracy and stability of the gas humidification unit. One possible solution would be to use real-time humidity measurement to determine the humidity of in-going and exiting gases. With a real-time measurement, it would be possible to minimize the errors caused by the fluctuation in the inlet humidities.

The humidities of exiting gases are measured and humidities of in-going gases are known from the calibration measurements,

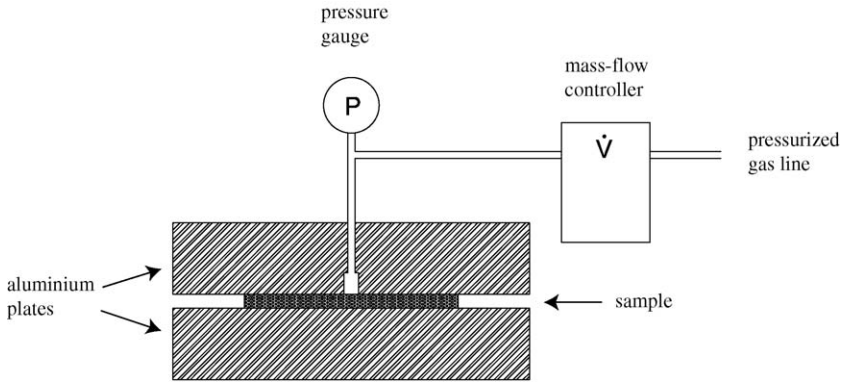

Fig. 4. Permeability measurement system.

Table 1
Measurement conditions and results of water transport measurements

Measurement	Dew-point side 1/side 2	Inlet c_{H_2O} (mol m^{-3})		outlet c_{H_2O} (mol m^{-3})		$\dot{m}_{H_2O}$ ($\times 10^{-4}$ kg m^{-2} s^{-1})
		Side 1	Side 2	Side 1	Side 2	
1	30/dry	1.83 ± 0.04	0	1.34 ± 0.07	0.48 ± 0.02	4.0 ± 0.5
2	33/dry	2.15 ± 0.04	0	1.51 ± 0.08	0.58 ± 0.03	5.2 ± 0.6
3	39/dry	2.95 ± 0.06	0	1.94 ± 0.10	0.93 ± 0.05	8.2 ± 0.9
4	43/dry	3.66 ± 0.07	0	2.17 ± 0.11	1.33 ± 0.07	11.9 ± 1.0
5	30/27	1.83 ± 0.04	1.36 ± 0.03	1.72 ± 0.09	1.62 ± 0.08	1.5 ± 1.0
6	33/27	2.15 ± 0.04	1.36 ± 0.03	1.89 ± 0.09	1.69 ± 0.08	2.5 ± 1.0
7	39/27	2.95 ± 0.06	1.36 ± 0.03	2.32 ± 0.12	1.95 ± 0.10	5.1 ± 1.3
8	43/27	3.66 ± 0.07	1.36 ± 0.03	2.73 ± 0.14	2.12 ± 0.11	7.1 ± 1.4
9	33/30	2.15 ± 0.04	1.66 ± 0.03	1.96 ± 0.10	1.84 ± 0.09	1.6 ± 1.1
10	39/30	2.95 ± 0.06	1.66 ± 0.03	2.44 ± 0.12	2.15 ± 0.11	4.2 ± 1.4
11	43/30	3.66 ± 0.07	1.66 ± 0.03	2.96 ± 0.15	2.16 ± 0.11	5.1 ± 1.5
12	39/33	2.95 ± 0.06	1.94 ± 0.04	2.48 ± 0.12	2.27 ± 0.11	3.4 ± 1.4
13	43/33	3.66 ± 0.07	1.94 ± 0.04	3.03 ± 0.15	2.32 ± 0.12	4.3 ± 1.6
14	43/39	3.66 ± 0.07	2.71 ± 0.05	3.36 ± 0.17	2.63 ± 0.13	1.0 ± 1.8
15	27	1.36 ± 0.03	1.36 ± 0.03	Only impedance measurement		
16	30	1.83 ± 0.04	1.83 ± 0.04	Only impedance measurement		
17	33	2.15 ± 0.04	2.15 ± 0.04	Only impedance measurement		
18	39	2.95 ± 0.06	2.95 ± 0.06	Only impedance measurement		
19	43	3.66 ± 0.07	3.66 ± 0.07	Only impedance measurement		
20	Dry	0	0	Only impedance measurement		

but the humidity profile inside the cell is not known. Therefore, only an averaged diffusion coefficient of water could be calculated directly from the measurement results. In order to take the water distribution into account, a model for transport phenomena inside the cell is needed. Such a model and more detailed analysis of measurement results are described in part II of this paper [1]. As a result of the modeling work, the dependence of the diffusion coefficient of water in the membrane on the water content was achieved.

3.2. Impedance measurements

The ac-impedance measurements were conducted under the same conditions as the water transport measurements. Additionally, impedance spectra were recorded under equal humidity conditions on both sides of the membrane. The measured frequency range was from 500 mHz to 200 kHz. The measurements were conducted in galvanostatic mode with 100 mA amplitude and the dc-level was set to 0 mA. Stray inductances were noticed to occur between the potential probes of the measurement device. Their effect was seen at high frequencies, i.e. the imaginary part of the impedance became positive at high frequencies. The upper frequency limit for fitting was set to 20 kHz in order to minimize the effect of inductances. The components of the equivalent circuit were fitted into the measurement results with the least squares method.

Recorded impedance spectra from constant humidity measurements (15–19) and also impedance curves calculated from their equivalent circuits are illustrated in Fig. 5. There were interferences in the impedance spectra 16–19 between 800 and 1000 Hz and those frequencies were not taken into account in the fitting procedure. There were significant differences between fittings and measurement results especially at frequencies close to the top of the high frequency arc. It resembles two semi-circles overlapping at high frequencies. The fitting error could be decreased by adding more components into the equivalent circuit, but this would have made the fitting procedure more challenging and initial guess dependent, and therefore these extra components were not added into the equivalent circuit.

The impedance curves of measurements 18 and 19 are practically identical. In these measurements the dew-point temperatures of in-going hydrogen were higher than the cell temperature and thus there was liquid water inside the cell. This means that the humidity conditions were similar in those measurements, because the water vapor was saturated.

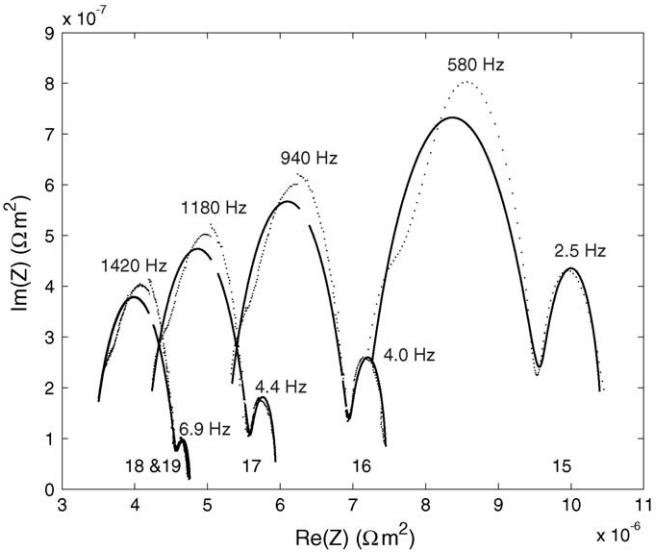

Fig. 5. Measured impedance curves from measurements 15–19 and corresponding fitted impedance curves from the equivalent circuits. Measurement results are marked with dots and impedance curves of equivalent circuits with solid line. The titles of the curves refer to the measurement conditions given in Table 1.

Table 2
Parameter values of the equivalent circuit fitted in the results of impedance measurements

Meas.	r_1 ($\times 10^{-6}\ \Omega\,m^2$)	r_2 ($\times 10^{-6}\ \Omega\,m^2$)	t_2 ($\times 10^3 s^{\alpha_2}\ \Omega^{-1}\,m^{-2}$)	α_2	c_2 ($F\,m^{-2}$)	r_3 ($\times 10^{-6}\ \Omega\,m^2$)	c_3 ($\times 10^4\ F\,m^2$)
1	19.77	4.50	2.80	0.573	106.6	1.324	10.36
2	18.98	4.87	3.84	0.531	115.6	1.328	10.62
3	11.17	3.40	4.12	0.547	123.2	1.052	11.60
4	7.92	2.04	3.92	0.584	127.8	0.641	14.18
5	6.89	1.27	2.36	0.672	135.0	0.381	19.80
6	6.25	1.15	2.14	0.681	128.4	0.343	20.36
7	5.33	0.98	2.08	0.692	130.6	0.260	20.18
8	5.23	1.03	2.44	0.669	125.8	0.292	22.54
9	7.19	1.33	1.98	0.680	119.8	0.445	18.06
10	4.20	0.75	1.76	0.724	142.8	0.159	31.84
11	3.84	0.71	2.06	0.698	121.4	0.123	38.74
12	4.05	0.81	2.38	0.679	124.6	0.146	38.34
13	4.03	0.82	2.46	0.676	123.8	0.148	36.90
14	3.93	0.84	3.14	0.647	121.4	0.101	49.42
15	7.09	1.29	2.52	0.657	127.4	0.398	18.94
16	5.22	0.89	1.56	0.722	124.6	0.242	22.18
17	4.12	0.76	1.80	0.714	127.0	0.166	29.46
18	3.38	0.61	2.02	0.707	125.8	0.083	41.62
19	3.39	0.61	2.06	0.710	133.8	0.078	41.98
20	630	Not reliable fitting results for other parameters					

The position of the curves is humidity dependent. The real part of the impedance of the left ends of curves, i.e. pure ohmic resistance between potential probes, varies from 3.4×10^{-6} to $7 \times 10^{-6}\ \Omega\,m^2$. This resistance is assumed to be caused by the membrane resistance, but it also includes the minor ohmic losses in the electrodes and contacts. The sizes of the arcs vary as a function of humidity, which implies that the kinetics of hydrogen adsorption/desorption and electron transfer reactions are also humidity dependent.

Fitted parameter values of all impedance measurements are given in Table 2 in area-specific form using the geometrical area of the cell. Electrode roughness, which is unknown, is not taken into account. It can be seen that the area-specific membrane resistance, r_1, reaches its maximum value when the in-going gas of side 2 is dry. In those cases, side 2 of the cell is humidified only by the diffusion of water through the membrane and therefore it remains quite dry even when there is liquid water at the side 1. There are some inconsistencies in the results of measurements 9 and 14. Value of r_1 from measurement 9 should be smaller than in the measurements 5, 6, 15 and 16, because of higher water content of the membrane. Value of r_1 from measurement 14 should be equal with measurements 18 and 19, because there was liquid water on both sides of the cell in those measurements. In the measurement 20, the membrane resistance was very high and it was not possible to get reliable fitting for other parameters.

The membrane conductivity can be calculated from the results of impedance data recorded under constant humidity conditions using the following equation

$$\sigma = \frac{l}{RA}$$

where l is the thickness, R the resistance, and A is the area of the membrane,. Area-specific membrane resistances, i.e. product of R and A are given in Table 2 as r_1. The use of this equation requires a constant conductivity of the membrane and therefore it can be used only with measurements where humidity conditions were similar on both sides of the cell. Membrane resistances under uneven humidity conditions are calculated in Part II of this work [1].

The calculated membrane conductivity is illustrated in Fig. 6 as a function of water vapor concentration and membrane water concentration. A linear fit was also made to the results, and the membrane conductivity as a function of water vapor concentration was found to be

$$\sigma = 1.95\ m^2\,mol^{-1}\,\Omega^{-1} \times c_{H_2O} \quad (4)$$

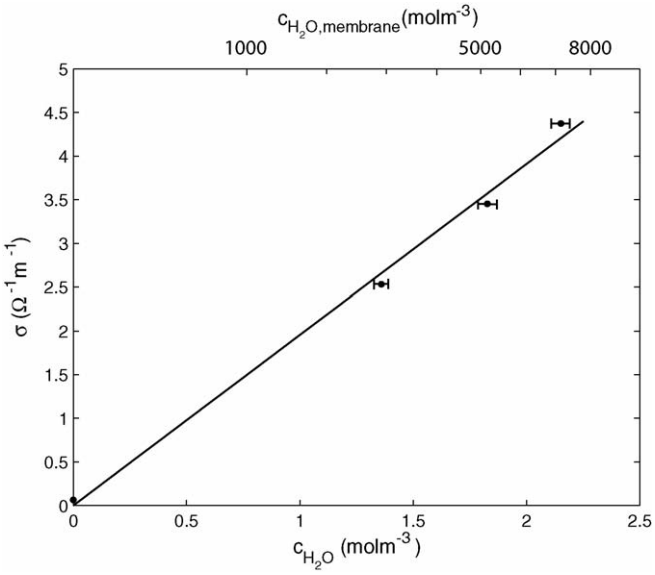

Fig. 6. Membrane conductivity as a function of water vapor concentration and water concentration in the membrane. Line is the linear fit calculated using Eq. (4).

or alternatively as a function of water concentration in the membrane

$$\sigma = 0.00065\,\mathrm{m^2\,mol^{-1}\,\Omega^{-1}} \times c_{\mathrm{H_2O,membrane}}. \quad (5)$$

The conductivity of the membrane stabilized with liquid water can be calculated from the results of impedance measurements 18 and 19 and it is $5.3 \pm 0.1\,\Omega^{-1}\,\mathrm{m}^{-1}$. This is in good agreement with the $5.2\,\Omega^{-1}\,\mathrm{m}^{-1}$ measured for 20 μm thick Gore-Select® membrane in Ref. [18]. Measurement 14 was neglected here, because its r_1-value differs significantly from measurements 18 and 19 due to some error in the measurements.

Linear dependence on the water vapor concentration was found for charge transfer resistance, adsorption/desorption resistance, and adsorption/desorption capacitance. Based on these measurements, constant phase element parameters, α_2 and t_2 had no clear dependence on the water concentration. Also the calculated double layer capacitance, c_2, appeared to be independent of the water concentration. However, at least c_2 should depend on the water vapor concentration, because water affects the electrical permittivity of the electrodes. More measurements are needed to find out these dependences.

The dependence of area-specific charge transfer resistance, r_2, on the water vapor concentration was found to be

$$r_2 = 2.2 \times 10^{-6}\ \Omega\,\mathrm{m^2} - 0.7 \times 10^{-6}\,\Omega\,\mathrm{m^5\,mol^{-1}} \times c_{\mathrm{H_2O}}. \quad (6)$$

The value of r_2 measured from the cell stabilized with liquid water is $0.61 \times 10^{-6}\,\Omega\,\mathrm{m^2}$. It seems that an increase in humidity decreases charge transfer resistance, i.e. the exchange current density increases with increasing humidity. One possible reason to this is the increased conductivity of proton conducting phase in the electrode.

The dependence of area-specific adsorption/desorption resistance, r_3, on the water vapor concentration is

$$r_3 = 0.8 \times 10^{-6}\ \Omega\,\mathrm{m^2} - 3.0 \times 10^{-7}\,\Omega\,\mathrm{m^5\,mol^{-1}} \times c_{\mathrm{H_2O}} \quad (7)$$

Based on these results, an increase in the water vapor concentration accelerates the surface reactions, i.e. humidity decreases the reaction resistance. The value of r_3 measured from the cell stabilized with liquid water is $0.80 \pm 0.05 \times 10^{-7}\,\Omega\,\mathrm{m^2}$.

Parameter c_3 is used to describe the capacitance of surface reactions and it increases as a function of water vapor concentration with the following dependence

$$c_3 = 6800\,\mathrm{F\,m^{-2}} + 128000\ \mathrm{F\ m\,mol^{-1}} \times c_{\mathrm{H_2O}}. \quad (8)$$

The value of c_3 measured from the cell stabilized with liquid water is $41.8 \pm 0.2 \times 10^4\,\mathrm{F\,m^{-2}}$.

3.3. Polarization measurements

The polarization curves of the H_2–H_2 cell were measured to obtain information about dc-operation of the cell and to cross-check the results of the impedance measurements. The polarization curves were measured after the water transport and impedance measurement series were completed. The polarization curves were measured under the same conditions as the impedance measurements 16–19. The polarization curves were measured from −0.5 to 0.5 A with 1 mA $\mathrm{s^{-1}}$ scan rate.

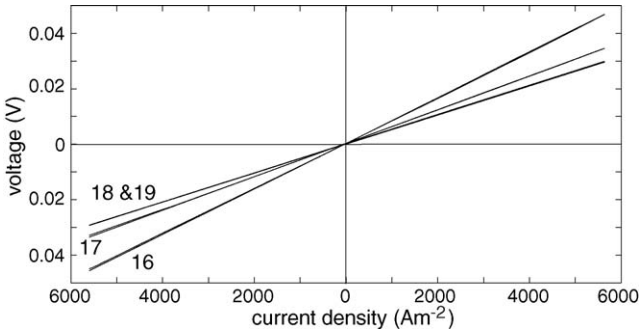

Fig. 7. Measured polarization curves of H_2–H_2 cell. Titles of curves refer to measurement conditions given in Table 1.

The measured polarization curves are illustrated in Fig. 7. In order to estimate the total area-specific cell resistance from the polarization measurements, a linear fit was made into polarization curves. The fitting results are given in Table 3. The total area-specific cell resistances calculated from the impedance measurements, i.e. the sum of membrane resistance r_1, twice the charge transfer resistance r_2 and twice the adsorption/desorption resistance r_3, are also given in Table 3.

The total area-specific cell resistances calculated from polarization curve and impedance measurements were similar. The differences between these methods are smaller than 10%, which shows that both methods can be used to determine total dc-resistance of H_2–H_2 cell.

3.4. Water uptake

A second order polynomial was fitted into the measurement results obtained with water vapor. The resulting equation for the WU isotherm at 35 °C is

$$\mathrm{WU} = 0.0012 - 0.00043 c_{\mathrm{H_2O}} + 0.014 c_{\mathrm{H_2O}}^2, \quad (9)$$

where $c_{\mathrm{H_2O}}$is the concentration of water vapor. Measurement results and the WU isotherm calculated with Eq. (9) are illustrated in Fig. 8.

Water uptake from the liquid water at 35 °C was measured to be 10%. Kolde et al. measured that the water uptake of 20 μm thick Gore-Select® membrane from liquid water is 32%, which is three times larger than the value measured here. The difference

Table 3
Calculated total area-specific cell resistances

Measurement	Area-specific resistance from polarization measurements ($\times 10^{-6}\,\Omega\,\mathrm{m^2}$)	Area-specific resistance from impedance measurements ($\times 10^{-6}\,\Omega\,\mathrm{m^2}$)
16	8.2	7.5
17	6.0	6.0
18	5.2	4.8
19	5.3	4.8

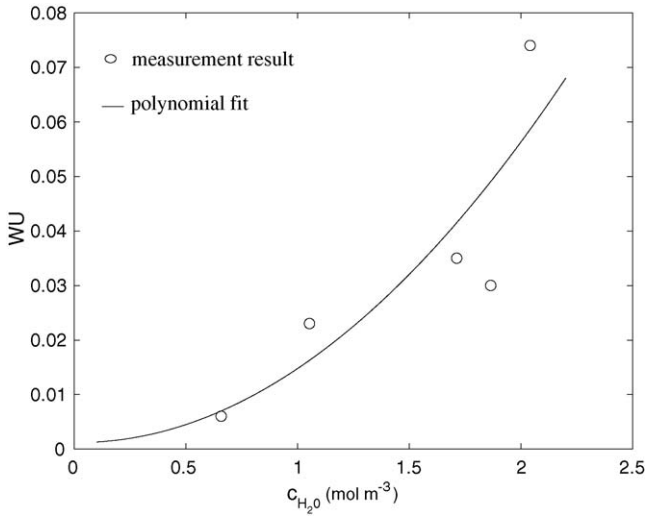

Fig. 8. Water uptake of GORE™ PRIMEA® Series 58 MEA at 35 °C as a function of water vapor concentration.

is very large and probably caused by the electrode layers or the difference in the removal of the surface water. Larger WU values can be easily obtained by different surface drying methods and therefore this measurement result can be highly inaccurate. There is no water condensation during the WU measurements from water vapor and therefore they should be more trustworthy.

3.5. Hydraulic permeability

Hydraulic permeability values and error estimates were calculated by fitting the Darcy's equation into the measurement results with the least squares method. The sample thicknesses, hydraulic permeabilities and error estimates for measured materials are given in Table 4. The electrodes were assumed to be incompressible in the calculation of hydraulic permeability. The pressure loss in the measurement system itself was measured by assembling the measurement system without a sample and it was found to be negligible compared to those with the samples and was thus ignored.

The permeability of the gas diffusion backing (GDB) was found to be strongly dependent on its thickness. Ihonen et al. [8] obtained a value of 3.3×10^{-11} m^2 for in-plane permeability of SGL ®Sigracet GDL 10-BA, but they used the thickness of uncompressed GDB in their calculations, even though the GDB was compressed in all of their measurements. The measured electrode permeabilities were the same in both measured cases, implying that the permeability of the membrane is significantly smaller than that of the electrodes, and the gas flow through and along the membrane can be neglected. This was an expected result, because Meier and Eigenberger [17] measured the hydraulic permeability of the Nafion® membrane to be of order 10^{-20} m^2, which is about seven orders of magnitude smaller than the measured permeability of the electrode.

Table 4
In-plane permeabilities and error estimates

Material	Thickness (μm)	Hydraulic permeability (m^2)
Steel net	440	$4.21 \pm 0.06 \times 10^{-10}$
SGL 10-BA	200 (compressed)	$1.06 \pm 0.03 \times 10^{-11}$
SGL 10-BA	250 (compressed)	$1.48 \pm 0.03 \times 10^{-11}$
SGL 10-BA	300 (compressed)	$2.40 \pm 0.03 \times 10^{-11}$
One electrode	10	$1.26 \pm 0.05 \times 10^{-13}$
Two electrodes	20	$1.28 \pm 0.06 \times 10^{-13}$

4. Summary and conclusions

A measurement system and technique for studying the properties of MEA using symmetrical hydrogen–hydrogen cell was presented. The measurements were made by controlling the humidities of ingoing hydrogen streams and measuring humidities of exiting hydrogen streams and impedance of the MEA. The measurement technique enables the determination of net water flux through the membrane, membrane conductivity and electrode kinetics under different humidification conditions. The MEA used in this work was Gore™ Primea® Series 58.

The net water flux through the membrane under different one- and two-phase conditions was calculated from the measurement results. As expected, the net water flux increased with increasing concentration difference of water over the membrane. The error estimates for net water fluxes were large and the accuracy of the measurements should be increased in further experiments, for example with longer measuring times.

The diffusion coefficient of water in the membrane cannot be calculated directly from the net water fluxes, because the transversal distribution of the water flux and concentration are not known. Therefore, modeling work is necessary to estimate the dependence of diffusion coefficient of water in the membrane as a function of water concentration. Analysis of water transport measurements with modeling approach is presented in part II of this paper [1]. Without modeling work, it would be possible to calculate only averaged diffusion coefficients.

The ac-impedance spectroscopy with H_2–H_2 cell was used to determine membrane conductivity and reaction kinetics of electrode reactions as a function of humidity. Polarization curves of the cell under different operating conditions were also recorded in order to validate the results of the impedance measurements.

The water uptake of the Gore™ Primea® Series 58 MEA from liquid water and from water vapor was measured at 35 °C. The water uptake from liquid water was noticed to be very sensitive for the removal of surface water. Hydraulic permeabilities of different cell components were also measured in order to obtain parameter values for the modeling work.

Acknowledgement

The financial support of the Academy of Finland (206132) is gratefully acknowledged.

Appendix A. Nomenclature

A	area (m^2)
c	concentration (mol m^{-3}) or area-specific capacitance (F m^{-2})
C	capacitance (F)

l thickness (m)
$\dot{m}$ mass flux ($kg\,m^{-2}\,s^{-1}$)
r area-specific resistance ($\Omega\,m^2$)
R resistance (Ω) or the molar gas constant ($8.314\,J\,mol^{-1}\,K^{-1}$)
t parameter of the constant phase element ($s^{\alpha}\,\Omega^{-1}\,m^{-2}$)
T temperature (°C or K)
WU water uptake
Z impedance (Ω)

Greek letters
α parameter of the constant phase element
σ conductivity ($\Omega^{-1}\,m^{-1}$)

Superscripts and subscripts
CPE constant phase element
DL double layer
H_2O-membrane water in the membrane

References

[1] O. Himanen, T. Hottinen, Electrochim. Acta, 2006, doi:10.1016/j.electata.2006.05.037.
[2] M. Ciureanu, S. Mikhailenko, S. Kaliaguine, Catal. Today 82 (2003) 195.
[3] N. Wagner, W. Schnurnberger, B. Müller, M. Lang, Electrochim. Acta 43 (1998) 3785.
[4] H. Matic, A. Lundblad, G. Lindbergh, P. Jacobsson, Electrochem. Solid-State Lett. 8 (2005) A5.
[5] R. Ströbel, M. Oszcipok, M. Fasil, B. Rohland, L. Jörissen, J. Garche, J. Power Sources 105 (2002) 208.
[6] J. Ihonen, F. Jaouen, G. Lindbergh, G. Sundholm, Electrochim. Acta 46 (2001) 2899.
[7] P. Gode, J. Ihonen, A. Strandroth, H. Ericson, G. Lindbergh, M. Paronen, F. Sundholm, G. Sundholm, N. Walsby, Fuel Cells 3 (2003) 21.
[8] J. Ihonen, M. Mikkola, G. Lindbergh, J. Electrochem. Soc. 151 (2004) A1152.
[9] O. Himanen, Master's Thesis, Helsinki University of Technology, Finland, 2003.
[10] http://www.drierite.com/, cited 27.7.2004.
[11] W. Ying, Y.-J. Sohn, W.-Y. Lee, J. Ke, C.-S. Kim, J. Power Sources 145 (2005) 563.
[12] T. Hottinen, O. Himanen, P. Lund, J. Power Sources 138 (2005) 205.
[13] E. Barsoukov, J. Macdonald, Impedance Spectroscopy, John Wiley & Sons Inc., USA, 2005, ISBN 0-471-64749-7.
[14] T. Pajkossy, Solid State Ionics 176 (2005) 1997.
[15] C. Hsu, F. Mansfeld, Corrosion 57 (2001) 747.
[16] M. Ciureanu, H. Wang, J. Electrochem. Soc. 146 (1999) 4031.
[17] F. Meier, G. Eigenberger, Electrochim. Acta 49 (2004) 1731.
[18] J. Kolde, M. Wilson, T. Zawodzinski, S. Gottesfeld, Proc. 1st International Symp on Proton Conducting Membrane Fuel Cells. Proc. – Electrochem. Soc., 95, 1995, p. 193.